Effects of the Presence or Absence of a Protein Corona on Silica Nanoparticle Uptake and Impact on Cells

Anna Lesniak,[†] Federico Fenaroli,[†,‡] Marco P. Monopoli, Christoffer Åberg, Kenneth A. Dawson,[*] and Anna Salvati[*]

Centre for BioNano Interactions, School of Chemistry and Chemical Biology, University College Dublin, Dublin 4, Ireland. [†]These authors contributed equally to this work. [‡]Present address: Department of Molecular Biosciences, University of Oslo, P.O Box 1041, Blindern, 0316 Oslo, Norway.

ABSTRACT

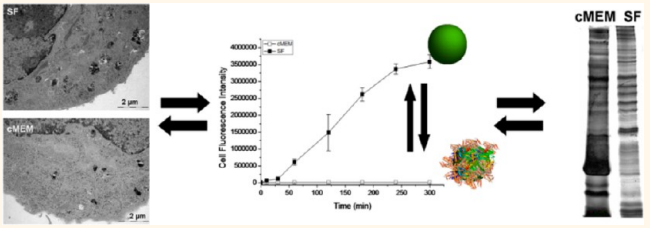

Nanoparticles enter cells through active processes, thanks to their capability of interacting with the cellular machinery. The protein layer (corona) that forms on their surface once nanoparticles are in contact with biological fluids, such as the cell serum, mediates the interactions with cells *in situ*. As a consequence of this, here we show that the same nanomaterial can lead to very different biological outcomes, when exposed to cells in the presence or absence of a preformed corona. In particular, silica nanoparticles exposed to cells in the absence of serum have a stronger adhesion to the cell membrane and higher internalization efficiency, in comparison to what is observed in medium containing serum, when a preformed corona is present on their surface. The different exposure conditions not only affect the uptake levels but also result in differences in the intracellular nanoparticle location and impact on cells. Interestingly, we also show that after only one hour of exposure, a corona of very different nature forms on the nanoparticles exposed to cells in the absence of serum. Evidence suggests that these different outcomes can all be connected to the different adhesion and surface properties in the two conditions.

KEYWORDS: nanoparticle · silica · serum free · protein corona · nanoparticle uptake · adhesion

Nanoscale objects interact with all components of living organisms, often in a manner that is fundamentally different from freely diffusing small molecules, on one hand, and large particles that are recognized by the immune system, on the other hand.[1−4] They possess an appropriate size to engage with the endogenous cellular machinery and can enter the cells through active energy-dependent processes.[5−12]

It is nowadays established, moreover, that the detailed nature of the surface of engineered nanoparticles once in contact with biological fluids (such as the serum), rather than its pristine surface, is the other determining factor in understanding their interactions with cells.[13−15] The corona is a very selective layer of proteins and other biomolecules, which strongly adsorbs on the nanoparticle surface for time scales longer than nanoparticle uptake in cells, thus constituting a new complex unit interacting with the cellular machinery.[16−22] The formation of a corona affects the material properties also by simply lowering the surface free energy of the bare material.

Here we show that for identical particles and cells, otherwise under identical conditions, the interactions with cells and the biological outcomes can vary greatly in the presence or in the absence of a preformed corona in serum. Several examples can be found, for different nanoparticles and cell systems, where uptake levels vary when particles are exposed to cells in serum-free medium or in the presence of a protein coating.[23−29] In particular, even though the details of the uptake mechanisms are still unresolved (indeed, details are still missing even for nanoparticles exposed to cells in the presence of serum),[30,31] it has been observed that nanoparticle uptake in serum-free conditions is, in most cases, higher than that measured for the same nanoparticle in the presence of serum[23−27] or a more simple protein solution (such as that observed for FePt nanoparticles in the presence of albumin or transferrin).[29] Moreover, different reports have shown that nanoparticle impact is also affected by the presence or absence of a protein coating (or other coatings) on their surface and that the presence of a corona in

* Address correspondence to Anna.Salvati@cbni.ucd.ie, Kenneth.A.Dawson@cbni.ucd.ie.

Received for review January 16, 2012 and accepted June 21, 2012.

Published online June 21, 2012
10.1021/nn300223w

the serum can mitigate the toxicity of the bare materials.[32−36]

In order to further explain and to connect these different outcomes, we have studied how uptake and the impact of silica nanoparticles in A549 lung epithelial cells are affected by the presence or the absence of a preformed corona in serum. When silica nanoparticles are exposed to cells in serum-free conditions, nanoparticle uptake is higher; moreover cellular damage is observed and nanoparticles free in the cytosol can be found. No signs of cell damage or particles free in the cytosol were observed for silica nanoparticles exposed to cells in the presence of serum. Here we show that the different efficiency of internalization and also final nanoparticle location and impact on cells all can be explained, at least in part, by the higher adhesion of the bare nanoparticles on the cell membrane when exposed to cells in the absence of serum.

Interestingly, we also show that even the (bare) nanoparticles added to cells in serum-free medium, after only 1 h in contact with cells, get coated by proteins and other molecules, and we have used mass spectrometry to clarify their origin. The identity of these proteins, many being proximate to the cell surface, but also intracellular, is also highly suggestive of strong and potentially disruptive interactions of the bare nanoparticles with the early processing and trafficking machinery of the cell.

Thus, for identical nanoparticles and cells, the biological outcomes are determined by the combined properties of nanoparticles and their adsorbed corona. Even though, given the high surface energy of nanoscaled objects, it is unlikely that the cellular machinery would interact with the pristine surface of the nanoparticles *in vivo*, this comparison helps to further clarify the importance of the layer of protein and biomolecules adsorbed on the nanoparticles in mediating the interactions of nanomaterials with cells. These differences should be kept in mind also when assessing nanoparticle impact on cells *in vitro*, when serum-free conditions are still commonly in use, and reports on particle impact and location may suggest conflicting outcomes for the same material because of the different exposure conditions investigated. The detailed identity of the adsorbed proteins can also modulate further nanoparticle uptake: for instance opsonin proteins, such as immunoglobulins and complement proteins, are known to affect particle uptake levels in specialized cells of the immune system, which recognize the opsonised particles and activate phagocytosis;[37−39] and it has been shown that even more subtle differences in protein composition, for example, complement depletion by heat inactivation of the serum, can affect particle uptake levels.[40] The implications are far-ranging, suggesting that the biological impacts of nanomaterials on organisms cannot be directly linked solely to the nature of the nanomaterial itself, but also to the nature of the particle−corona complexes, and efforts to correlate outcomes only with the pristine nature of the material will be limited.

TABLE 1. Physicochemical Characterisation of the Nanoparticles and Their Dispersions in Relevant Media[a]

	50 nm silica		
dispersant	water	PBS	cMEM
z-av (*d*, nm)[b]	49	66	
polydispersity index[c]	0.02	0.2	
size (*d*, nm)[d]			105
zeta potential (mV)		−20	−8
mobility (μm cm/(V s))		−1.5	−0.6
conductivity (mS/cm)		17	15

[a] Nanoparticle size and size distribution were determined by dynamic light scattering in water, phosphate saline buffer (PBS), and complete cell culture media (cMEM). All measurements were performed at 25 °C at 25 μg/mL. Zeta potential was measured in PBS and cMEM. [b] *z*-average hydrodynamic diameter extracted by cumulant analysis of the data. [c] Polydispersity index from cumulant fitting. [d] Average hydrodynamic diameter determined from the size distribution obtained by analyzing the data using the CONTIN algorithm. A smaller peak of objects around 10 nm was also given, probably due to small protein aggregates.

RESULTS AND DISCUSSION

Fluorescently labeled silica nanoparticles (50 nm) were dispersed in serum-free MEM medium (SF) and complete medium supplemented with 10% serum (cMEM). The dispersions in water, in phosphate buffer saline, and in these two media were characterized in order to determine nanoparticle size, polydispersity, and zeta potential in the relevant conditions.

Table 1 summarizes the results at room temperature and suggests a good control of the nanoparticle dispersion. A more extensive characterization of the same dispersion in cMEM and its stability at 37 °C at different times was published in a previous study[9] and also showed that the size distribution shifted to higher values due to protein adsorption on the nanoparticles. Overall, the dispersion was stable in the conditions applied for cell culture studies and for the full length of the experiments.

In order to check further for nanoparticle stability in serum-free conditions, a similar study has been performed here, for the 50 nm particles, as a function of time in serum-free MEM. The results are presented in Table 2 and indicated that the dispersion was stable for up to 300 min, also in serum-free medium at 37 °C. These results collectively indicated a good control of nanoparticle dispersions under all the applied conditions.

Similar dispersions were prepared also for 40 nm carboxylated polystyrene nanoparticles in SF and cMEM, and a panel of different cell types, including lung epithelial A549 cells, cervix epithelium HeLa cells, glial astrocytoma 1321N1 cells, and brain capillary

endothelial *hCMEC*/D3 cells, was tested with the two nanoparticle types, in both SF and cMEM, in order to determine the effect of the presence or absence of a preformed corona on nanoparticle uptake levels. It has to be pointed out that the uptake in serum-free conditions was performed without any preincubation in serum-free medium, in order to exclude starvation effects—at least at early stages of uptake—and only with the purpose of studying how uptake efficiency and impact can vary when nanoparticles are covered or not by a corona, prior to their interaction with cells. Thus, we prefer to focus the discussion here mainly on the internalization efficiency at the earlier exposure times, which were already indicative of a significant difference for the serum-free exposure scenarios (results at longer exposure times were in agreement with observations at earlier times, as suggested by the uptake kinetics presented in Figure 1).

Higher uptake levels in SF were observed for all the different cell lines investigated and even when comparing the uptake of polystyrene nanoparticles in complete and serum-free conditions (see Supplementary Figure S1). Thus, even though we cannot exclude that different nanoparticle−cell systems may behave differently (for instance cells of the immune system,

TABLE 2. Stability of the Nanoparticle Dispersion in Serum-Free Conditions[a]

	50 nm silica				
time	0 min	10 min	120 min	300 min	1440 min
z-av (*d*, nm)[b]	64	55	44	40	
polydispersity index[c]	0.14	0.12	0.08	0.19	
size (*d*, nm)[d]					258

[a] DLS measurements of 25 μg/mL 50 nm silica nanoparticles in serum-free MEM after mixing (time zero) and at 37 °C, as a function of time. [b] *z*-average hydrodynamic diameter extracted by cumulant analysis of the data. [c] Polydispersity index from cumulant fitting. [d] Average hydrodynamic diameter determined from the size distribution obtained by analyzing the data using the CONTIN algorithm.

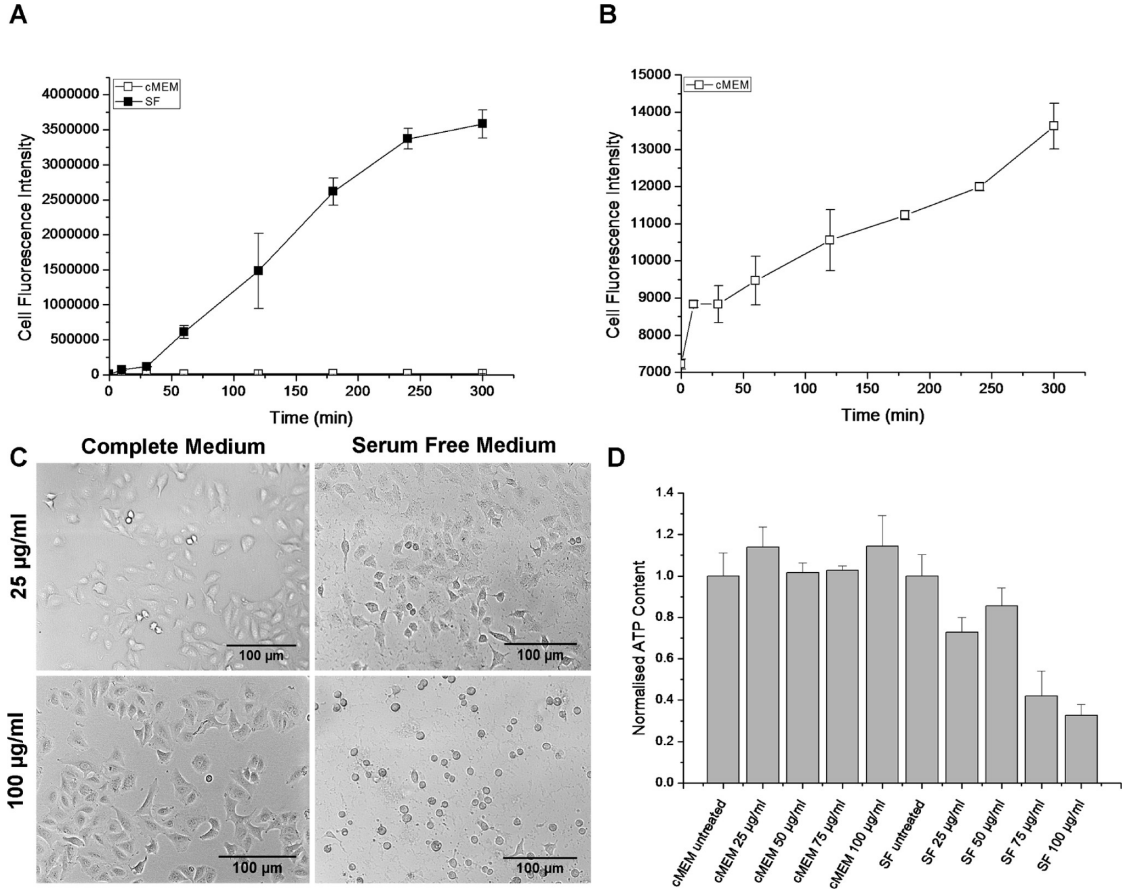

Figure 1. (A) Kinetics of uptake of 25 μg/mL fluorescently labeled 50 nm silica nanoparticles in complete medium (cMEM, empty symbols) and serum-free medium (SF, filled symbols) by A549 cells, as determined by flow cytometry. Error bars are the standard deviation of the mean cell fluorescence intensity averaged over 3 replicates. (B) Curve in complete medium (from panel A) alone. (C) Phase contrast images of A549 cells exposed for 2 h to 25 and 100 μg/mL of 50 nm silica nanoparticles in cMEM and SF. Several cells assumed a spherical shape after exposure to silica nanoparticles in serum-free medium (the effect was proportional to nanoparticle concentration). The same was not observed in cells grown in only SF or cells exposed to the same nanoparticles in cMEM. (D) ATP levels of untreated A549 cells and A549 cells exposed to different doses of 50 nm silica nanoparticles in cMEM and SF for 24 h, after normalization for the ATP content of untreated cells in the same conditions. A decrease of ATP levels was detected for cells exposed to nanoparticles in serum-free conditions. Error bars are the standard deviation of the average over 3 replicates.

specialized in removal of opsonized particles or primary cells), this observation did not depend on a specific nanoparticle−cell combination (at least for the cases investigated).

In order to further investigate these differences, we have focused the work on the biological outcomes observed for silica nanoparticles in lung epithelial A549 cells, as a common model cell line, often applied in several similar studies.[1,9,26,40−44] Figure 1 shows a comparison of the kinetics of uptake of silica nanoparticles in A549 cells in serum-free and complete media, obtained by flow cytometry, as described in the Methods. As anticipated in Supplementary Figure S1, the kinetic study also clearly indicated that uptake was always higher when the nanoparticles were exposed to cells in SF.

We have shown previously that a very good control of nanoparticle exposure and accumulation profiles could be obtained for these nanoparticles in cMEM.[9] Although we did not observe nanoparticle agglomeration (Table 2), at least in the first 6 h, this was not the same in serum-free conditions, and even if in all cases the uptake in serum-free conditions was higher than in cMEM, the internalization levels were very difficult to reproduce quantitatively in independent experiments.

Phase contrast images (also in Figure 1) of the cell cultures exposed to silica nanoparticles in cMEM and SF also indicated that, in several cases, cells exposed to silica in serum-free conditions changed their phenotype and assumed a spherical shape, indicative of loss of cell adhesion and cell damage. The extent of this effect was not always the same, and in some cases it was possible to expose the cells in serum-free conditions for up to 24 h without such strong impact. ATP measurements of cells exposed to different concentrations of silica in cMEM and SF (also in Figure 1) confirmed a dose-dependent decrease of cell viability in cells exposed to the nanoparticles in serum-free conditions. Even though the applied doses were all relatively high, these results clearly indicated that the nature of interactions of the same material in the presence or absence of proteins was very different.

In order to prove that the different uptake levels were related to the presence of proteins on the nanoparticles prior to addition to cells, silica nanoparticles were dispersed in serum to allow the formation of a protein corona, followed by hard corona nanoparticle complex isolation and redispersion in serum-free medium (see the Methods for details): the results (Supplementary Figure S2) showed that the uptake levels of the corona nanoparticle complexes were much lower than when adding the bare particles in serum-free medium, thus confirming that the higher uptake for bare particles in serum-free conditions was due to the absence of proteins on the nanoparticles at the moment of exposure. Moreover phase contrast images showed no strong changes of cell phenotype in these conditions, and this suggested that the damage observed for bare particles in serum-free medium was connected to the different interaction of the particles with the cell membrane, rather than the absence of proteins in the medium.

To further understand the different behavior, confocal and electron microscopy (EM) were combined to investigate nanoparticle intracellular localization. A detailed time- and space-resolved analysis on the nanoparticle distribution inside the cells in cMEM was reported elsewhere.[9] Extensive EM analysis was performed here to compare intracellular load and location in cMEM and SF. Some representative EM images are shown in Figure 2.

The results confirmed that nanoparticles were internalized by the cells also in serum-free conditions. A first observation clearly confirmed that uptake in cells exposed to nanoparticles in SF was higher than in cMEM, at the same exposure times. This was more evident at earlier times, where only a few particles could be seen in cells treated in cMEM (see also Shapero[9] for more details), while in contrast cells exposed to silica in SF showed a substantial number of internalized nanoparticles. Moreover, while in complete medium nanoparticles were always seen enclosed in vesicles along the endolysosomal pathway; in serum-free medium, together with nanoparticles engulfed in vesicles and in lysosomes, we also found nanoparticles that seemed to be free in the cytosol (or anyway, in these cases, it was very difficult to recognize the presence of a lipid bilayer enclosing the nanoparticles in some organellar structure).

We also noted that, after nanoparticle treatment in serum-free conditions, in many cases a large amount of nanoparticles clustered in proximity of the plasma membrane was present, even after all the washing steps needed for sample preparation (see Methods for details). An example of this is shown in Figure 2E, where one can also note the transversal sections of cell filopodia around those clusters. A first possible explanation of this observation could be nanoparticle agglomeration in SF; however the data in Table 2 indicated no agglomeration, at least for the first 6 h. Possibly these cell protrusions were strongly interacting with the nanoparticles and created some entanglements around the cell surface, in which nanoparticles remained trapped. Similar events were rare in cells treated with nanoparticles in cMEM.

A series of details of typical nanoparticle locations inside the cells at larger magnification is given in Figure 3 for cells treated for different times with 25 and 100 μg/mL silica nanoparticles in SF.

The time-resolved electron microscopy analysis showed that in serum-free conditions for the lower concentration and shorter incubation times silica

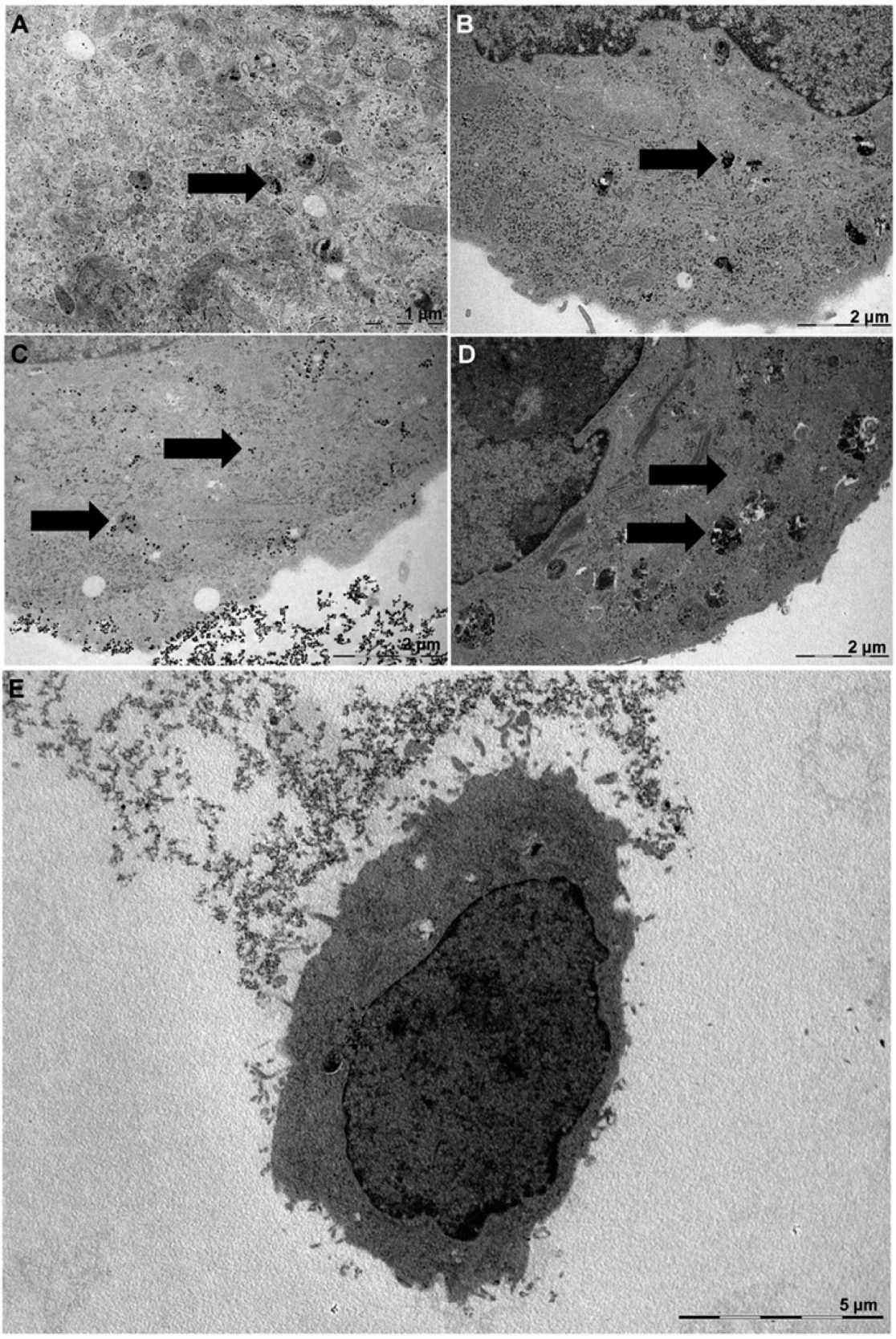

Figure 2. Transmission electron microscopy images of A549 cells exposed to 100 μg/mL 50 nm silica nanoparticles in complete and serum-free medium for 4 h (A and C, respectively) and 24 h (B and D, respectively). (E) Low-magnification image of a typical A549 cell after nanoparticle treatment in serum-free medium. The arrows indicate some of the NPs in the cells.

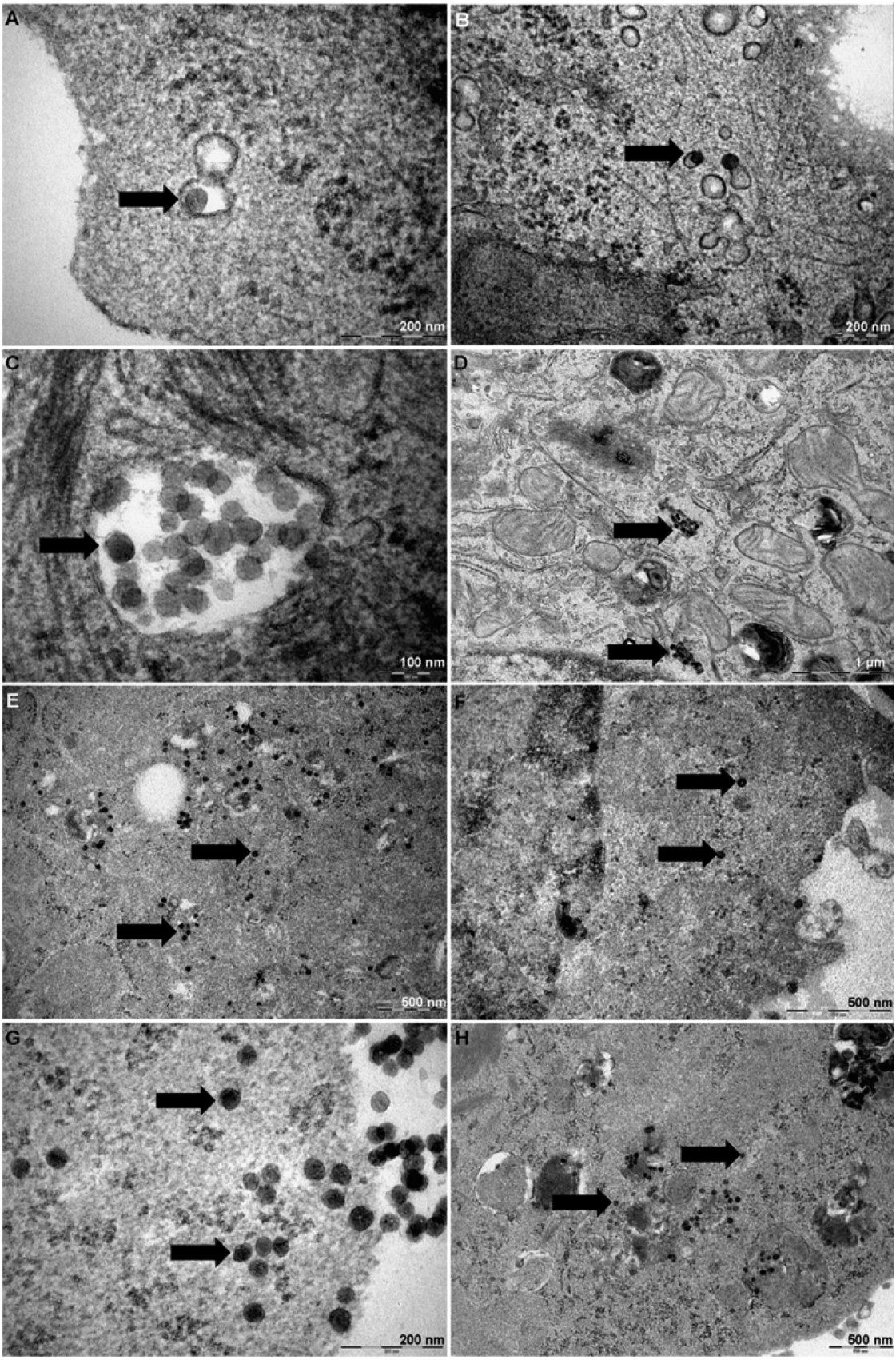

Figure 3. Details of typical nanoparticle intracellular locations: representative images from cells exposed to 25 (A–F) or 100 (G, H) μg/mL silica in serum-free medium. (A, B) Nanoparticles enclosed in vesicles close to the cell membrane, (C) inside an early endosome, and (D) inside a late endosome or a lysosome. For longer exposure times (E, F: 24 h) or also when treating cells with higher nanoparticle concentrations (G, H), nanoparticles free in the cytosol were observed. The arrows indicate some of the NPs in the cells.

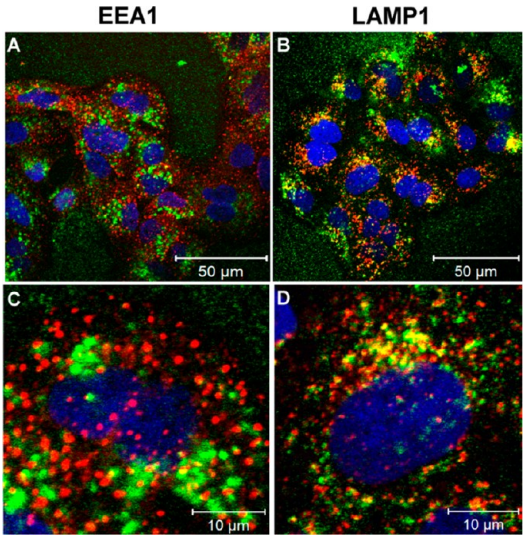

Figure 4. Confocal images of A549 cells treated for 24 h with 100 μg/mL green 50 nm silica nanoparticles in serum-free medium. In red: EEA1 staining of the early endosomes or LAMP1 staining of the lysosomes (secondary antibody conjugated with Alexa-647). (A, B) Low magnification. (C, D) Enlarged details of single cells in the same conditions. Blue: DAPI-stained nuclei.

nanoparticles were mainly found engulfed in vesicles (such as in cMEM)[9] along the endolysosomal pathway. Nanoparticles free in the cytosol were also observed (most of them closer to the cell membrane, as in the images in Figure 3), especially at longer exposure times or at higher nanoparticle concentration. This leaves open the possibility for multiple entry pathways, but it could be simply explained as a consequence of the cell damage that we observed in these conditions. Again, we stress that we never saw similar behavior when exposing cells in cMEM, where also no cell damage, in fact, was observed (see Figure 1C), and in that case nanoparticles of this size were always found enclosed in vesicles or in some organelle.

With confocal microscopy (Figure 4) we could confirm by immunostaining that the major final localization of the nanoparticles was in the lysosomes, as in cMEM conditions.[9] This was particularly clear after long exposure time (24 h), where a high level of colocalization could be seen with lysosomal marker (LAMP1) positive structures, even though in these conditions not all of the nanoparticles were (yet) found there. This could also be related to the presence of nanoparticles that seemed free in the cytosol at EM analysis. Moreover, confocal imaging confirmed the presence of residual clusters of nanoparticles out of the cells (and also on the glass slide) in serum-free conditions, as it was noted also by EM. This potentially could affect the flow cytometry data and explain the difficulty in reproducing quantitatively the uptake profiles, as discussed earlier. Regardless of this potential limit of flow cytometry (and confocal imaging), EM analysis clearly confirmed the general observations of higher intracellular load in cells exposed to the nanoparticles in SF.

In order to study whether nanoparticle uptake in SF was energy dependent, cells were exposed to silica in serum-free conditions after depletion of energy, using sodium azide, or after incubation at 4 °C, which affects the activity of many proteins and also the fluidity of the lipid membrane. Cell fluorescence was then measured by flow cytometry (see Supplementary Figure S3), and, as we demonstrated for cells exposed to silica in cMEM, also in serum-free conditions we could detect a decrease of nanoparticle uptake in energy-depleted cells. We may conclude that uptake was an energy-dependent process; however the extent of the decrease was not as strong as when performing the same experiment in cMEM.[9] Further EM and confocal imaging clearly explained this difference (also in Supplementary Figure S3). There, it was possible to see that in serum-free conditions large clusters of nanoparticles were present on the cell membrane, and this could affect the flow cytometry results. EM however left no doubt on the energy-dependent nature of the uptake of nanoparticles in serum-free conditions: no nanoparticles could be found in cells exposed at 4 °C, neither in vesicles nor free in the cytosol. In rare cases, only a few nanoparticles were found when cells were treated by sodium azide.

Having excluded nanoparticle agglomeration (see Table 2) and the presence of portals of entry that do not require energy expenditure when exposing cells to nanoparticles in serum-free conditions, as in all the experiments presented here we noted a higher amount of nanoparticles adhering outside the cell membrane (as well as on the glass slides), we hypothesized that a stronger adhesion on the cell surface (and filopodia) in serum-free conditions could be the explanation (at least in part) for the higher degree of uptake. In order to evaluate and confirm this hypothesis, cells were incubated at 4 °C with the nanoparticle dispersions in cMEM and SF for different lengths of times, in order to let the nanoparticles adhere on the cell surface without nanoparticle uptake (as shown earlier). Then the nanoparticle dispersion was replaced, after a few washes with PBS, by nanoparticle-free cMEM, and the cells were warmed at 37 °C and grown for a further 3 h to allow all the nanoparticles adhered on the cell surface to be internalized and quantified by flow cytometry. This allowed us to study nanoparticle adhesion to the cell membrane (in conditions in which nanoparticle uptake is shut down) and its effects on nanoparticle internalization efficiency, and to exclude the potential presence of residual nanoparticles outside the cell membrane, which could affect the flow cytometry fluorescence levels. The results, which are shown in Figure 5 (see also Figure S4), clearly confirmed that indeed nanoparticles in serum-free conditions had a stronger adhesion on the cell surface,

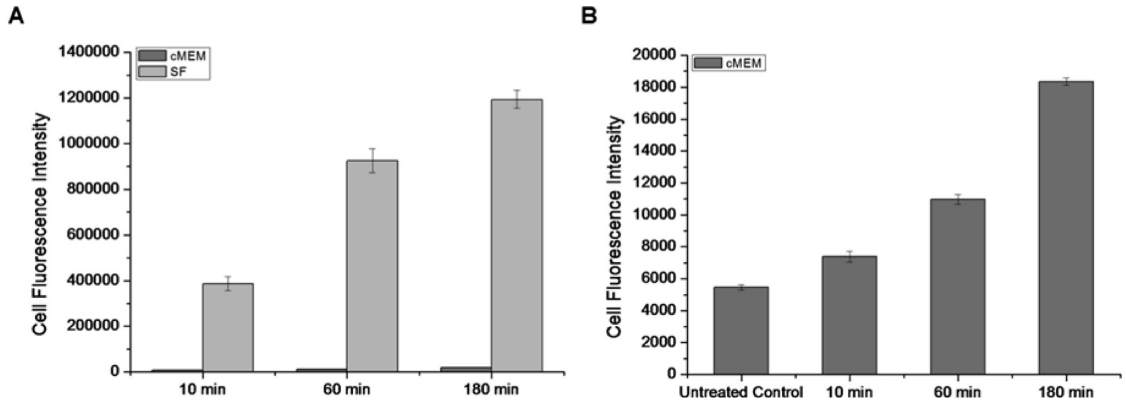

Figure 5. Adhesion of 50 nm silica nanoparticles on the cell membrane of A549 cells in serum-free (SF) and complete medium (cMEM). Nanoparticles (100 μg/mL) were exposed to A549 cells at 4 °C for different times in order to prevent nanoparticle uptake (also shown in Figure S3) and allow them to adhere to the cell membrane. The nanoparticle dispersion was then replaced by complete medium without nanoparticles, and cells were warmed to 37 °C and grown for a further 3 h prior to flow cytometry assessment of internalized nanoparticle levels (see Methods for more details). Error bars are the standard deviation of the mean cell fluorescence intensity averaged over 3 replicates. (B) Results in cMEM from panel A and the background fluorescence of untreated control cells.

while the presence of proteins on the nanoparticles, such as after incubation in cMEM, strongly reduced the initial adhesion, and this resulted in a lower internalized dose.

Although this observation is totally independent from the mechanism of uptake that particles could exploit in the two cases, it could contribute, at least in part, to the explanation of such a difference. We found similar conclusions when exposing polystyrene nanoparticles to serum of different compositions, which resulted in a different amount of proteins bound on the nanoparticle surfaces.[40] There we also found that the nanoparticles with the smaller protein coverage showed a higher uptake in cells, even if the effect was much more subtle than the one outlined here for the more extreme case of serum-free exposure.

Finally, since even in serum-free conditions we cannot fully exclude the presence of proteins on the nanoparticles, because of the very high surface energy of the bare material and the observed strong interactions with the cell membrane, SDS PAGE was used to detect the presence of a corona on the nanoparticles recovered from cell cultures exposed to 50 nm silica in serum-free MEM. Thus, cells were exposed to the nanoparticles in serum-free MEM, as in previous studies, and after only 1 h in contact with cells, the extracellular nanoparticles were recovered, in order to investigate whether proteins were present on their surface already after such a short time. The result is shown in Supplementary Figure S5 and confirmed, as expected, that proteins adsorbed on the nanoparticles could be found even on nanoparticles originally added to cells in serum-free conditions. In order to clarify their nature and origin, mass spectrometry has been used for their identification. A list of the most abundant proteins that were recovered on the nanoparticles exposed to cells in SF is given in Table 3 (more details can be found in Supplementary Figure S6 and Supplementary Table 1).

A corona of very different nature was found on the particles recovered from cells exposed in the absence of serum in the medium. While in complete medium the major components of the corona were immunoglobulin, complement proteins, and apolipoproteins (see Supplementary Table 1), as observed in similar studies for similar materials dispersed in serum and plasma,[45,46] the most abundant proteins that adsorbed on the nanoparticles exposed to cells in serum-free conditions were mainly cytosolic proteins, components of the cytoskeleton, and proteins normally associated with the cell membrane. These results can be related, again, to the strong adhesion of the bare silica on the cell membrane in serum-free conditions and are indicative of cell damage even after only 1 h of exposure. Interestingly, almost none of these proteins could be found on the nanoparticles exposed to cells in complete medium (see comparison of their spectral counts, SpC, in Table 3), and this is another example that shows that the nature of the protein layer adsorbed on the nanoparticles is strongly dependent on the conditions in which nanoparticles are found *in situ*.

Moreover, while the protein corona formed in serum is normally composed of only 200−300 different proteins,[45,46] it is interesting to note that for the particles recovered from cells in SF we could identify more than 800 proteins (or roughly 600 if excluding the proteins with very low signal). This is probably due to the lower concentration of proteins in the recovered serum-free medium (compared to the protein concentration in serum or, in this case, the cMEM), thus a lower competition for the nanoparticle surface.

TABLE 3. List of the Most Abundant Proteins Identified by Mass Spectrometry on 50 nm Silica Nanoparticles (100 μg/mL) Recovered from Cell Cultures Exposed for 1 h in SF[a]

accession			SpC sf	SpC cMEM	
RSp	name	MW	human	human	cellular component/function
P21333	filamin-A	280 561.4	137	40	cytoplasm and cytoskeleton, links actin filaments to membrane glycoproteins
O75369	filamin-B	277 987.3	125		cytoplasm and cytoskeleton, connects cell membrane constituents to the actin cytoskeleton
P14618	pyruvate kinase isozymes M1/M2	57 900.17	91	63	cytoplasm and nucleus, glycolytic enzyme
O43707	alpha-actinin-4	104 788.5	76		cytoplasm and nucleus, protein transport, regulation of apoptosis
P00352	retinal dehydrogenase 1	54 826.99	65		cytoplasm, binds free retinal
Q13813	spectrin alpha chain, brain	284362.5	65		cytoplasm and cytoskeleton, structural constituent of cytoskeleton
P35579	myosin-9	226 390.6	56	70	cell shape, play role in cytokinesis
P12814	alpha-actinin-1	102 992.7	55		cell membrane, cell projection, cytoplasm, cytoskeleton, membrane, focal adhesion assembly, regulation of apoptosis
Q00610	clathrin heavy chain 1	191 491.7	54		coated pit, cytoplasmic vesicle, membrane, major protein of coated pits and vesicles
Q01082	spectrin beta chain, brain 1	274 437.2	53		cell membrane, cytoplasm, cytoskeleton, membrane, actin filament capping
P11413	glucose-6-phosphate 1-dehydrogenase	59 219.09	46		centrosome, cytosol, internal side of plasma membrane, intracellular membrane-bound organelle, carbohydrate and glucose metabolism
Q71U36	tubulin alpha-1A chain	50 103.65	39	19	major constituent of microtubules, cytoplasm, cytoskeleton
Q9Y490	talin-1	269 596.3	39	238	cell membrane, cytoplasm, cytoskeleton
P53396	ATP-citrate synthase	120 762.1	38		cytoplasm, nucleus lipid synthesis, ATP binding, ATP citrate synthase activity
P68104	elongation factor 1-alpha 1	50 109.18	38	30	cytoplasm and nucleus
P69905	hemoglobin subunit alpha	15 247.92	38	34	oxygen transport from the lung to the various peripheral tissues
P29401	transketolase	67 834.88	35		cytosol, transferase, involved in energy reserve metabolic process
P10809	60 kDa heat shock protein, mitochondrial	61 016.47	34	6	mitochondrion, mitochondrial protein import and macromolecular assembly
P13639	elongation factor 2	95 277.08	34	15	cytoplasm, cytosol and ribonucleoprotein complex, protein biosynthesis, GTP-binding, nucleotide-binding
P07355	annexin A2	38 579.82	33	1	basement membrane, extracellular matrix, secreted, positive regulation of vesicle fusion
Q15149	plectin 3	531 465.9	32		cell junction, cytoplasm, cytoskeleton, cellular component disassembly involved in apoptosis
O60701	UDP-glucose 6-dehydrogenase	54 989.33	31	13	cytosol, biosynthesis of glycosaminoglycans
P04083	annexin A1	38 690	30		cell membrane, cell projection, cilium, cytoplasm promotes membrane fusion and is involved in exocytosis
P60842	eukaryotic initiation factor 4A-I	46 124.6	29	3	cytosol, eukaryotic translation protein biosynthesis
Q14204	cytoplasmic dynein 1 heavy chain 1	532 071.8	29	9	cytoplasm, cytoskeleton, dynein, microtubule transport, microtubule-based movement

[a] The mass spectrometry data (from the gel in Supplementary Figure S6) have been searched against Swiss-prot human and bovine databases and ranked according to their total spectral counts, as detailed in the Methods. The table shows the most abundant human proteins in the corona formed on the particles in SF with their spectral counts (SpC SF human) and the spectral counts of the same proteins in the corona in cMEM (SpC cMEM human). The main protein location and function in the cell is also indicated (from Uniprot database), together with the accession number (accession, RSp, also from Uniprot database) and the protein molecular weight (MW).

CONCLUSIONS

Different reports have shown that for several nanoparticle−cell systems nanoparticles exposed to cells in serum-free conditions can enter cells with higher efficiency than when they are covered by a corona in biological fluids. Even though we cannot exclude that other cell−nanoparticle systems may behave differently (for instance cells of the immune system specialized in phagocytosis and clearance of particles coated by opsonins), here we showed that silica nanoparticles are internalized very differently (both in degree and in processes) when they are exposed to A549 cells in complete medium or in serum-free conditions, likely by a variety of routes, but all underpinned by the fact that direct physical associations between cell and nanoparticles are much stronger for the bare surfaces. The accumulation in serum-free medium was higher and resulted in nanoparticles accumulating in the lysosomes (as in complete medium), but also some nanoparticles which seemed to be free in the cytosol, something that we never observed in the presence of a well-developed corona in serum. At least a significant portion of the uptake was however still energy dependent, as it was also in complete medium. Clearly nanoparticles in serum-free conditions showed a higher degree of adhesion on the cell membrane. This initial stronger adhesion could, at least in part, contribute to the higher uptake efficiency. Consistently, quantitative uptake results were more difficult to obtain, and there was evidence of cellular damage and particles free in the cytosol. This is of some importance, as it suggests that there is a need to be cautious in interpreting *in vitro* observations, in which

nanoparticles are reported to be free in the cytosol, as this may be caused by damage of the early uptake pathway when exposing nanoparticles to cells in the absence of serum, rather than an endogenous regulated cellular process.

Indeed, particles exposed to cells in serum-free conditions, recovered from the extracellular medium after only 1 h exposure to cells, possessed a new kind of adsorbed layer: in this case, the corona was composed of proteins close to the cell surface and of the cytoskeleton, but also of cytosolic proteins (presumably several membrane lipids could also be found), as a consequence of the stronger adhesion to the cell membrane and the resulting cell damage, all again in distinction from those cases where a preformed corona was present in serum. While the details of all these processes may be poorly understood, the basic principles are significant for future studies.

Thus, in realistic situations, it will be usual that nanoparticles will be exposed to biological fluids before contact with the cellular machinery, and this layer limits the disruptive nature of the interactions and thereby mitigates acute cellular toxicity. Nanoparticles exposed to cells in the absence of proteins in the medium interact strongly with the early processing and trafficking machinery of the cell, thereby lowering their surface free energy by adsorption of biomolecules from those systems. Since (as usual for the hard corona) this adsorption process, when complete, is essentially irreversible, the composition of the "corona" derived from contact with the cell is enriched in the molecules with which nanoparticles come in early contact. In essence, if the surface energy of the bare nanoparticles is not reduced by formation of a corona from biomolecules in the medium, then it will use cellular components to form one.

Succinctly put, one can obtain a wide range of outcomes simply by changing the environment (and thereby the corona),[19,32,33,40] and one must, in the future, consider nanoparticle−medium−cell systems as single entities. At the practical level, this could lead to apparent differences in reports of nanoparticle toxicity for the same nanomaterial, if different conditions are applied, potentially confounding efforts to obtain reproducible agreeing outcomes. These comments pertain also to dispersions for *in vivo* studies, where some evidence suggests different acute outcomes depending on the nature of the starting dispersion. Other differences could arise when comparing *in vivo* and *in vitro* findings, where protein concentrations (thus the resulting corona) can also be very different,[19] and this could also affect biological outcomes.

This suggests that one should consider carefully the nature of the dispersion medium, not just from the point of view of the quality of the dispersion but also for the potential of inducing cellular effects.

METHODS

Nanoparticle Characterization. Yellow-green silica (SiO_2) nanoparticles (50 nm) were purchased from G. Kisker-Products for Biotechnology (Steinfurt, Germany) (the fluorescent dye in these particles is chemically linked in the core during particle synthesis). Nanoparticle size measurements by dynamic light scattering (DLS) were carried out in water, phosphate buffered saline (PBS), serum-free minimum essential medium (SF), and the complete cell culture medium (cMEM), consisting of MEM, supplemented with 10% fetal calf serum (Gibco), 1% penicillin/streptomycin (Invitrogen Corp.), and 1% MEM nonessential amino acids (HyClone). Nanoparticle dispersions were prepared by diluting the nanoparticle stock to the required concentration in SF or cMEM. Measurements were performed at 25 °C (Table 1) and 37 °C (Table 2), using a Malvern Zetasizer Nano ZS90 (Worcestershire, UK). DLS results are reported as the average of at least 3 runs, each containing 100 individual measurements. Zeta potential was measured, on the same instrument, in PBS and cMEM. Selected experiments were performed with 40 nm yellow-green carboxylated polystyrene nanoparticles (Invitrogen). Their characterization in the same media is reported elsewhere.[1,40,42]

Cell Culture. A549 cells (original batches from ATCC, item number CCL-185) were cultured at 37 °C in 5% CO_2 in cMEM, prepared as described above. Human glial astrocytoma 1321N1 cells (passage 2−10) and human cervix epithelium HeLa cells (passage 5−10) were cultured at 37 °C in 5% CO_2 in Dulbecco's modified Eagle's medium (DMEM) supplemented with 10% fetal bovine serum and 1% penicillin/streptomycin. Human brain capillary endothelial *hCMEC*/D3 cells were obtained from Florence Miller and B.B. Weksler (INSERM, France) and were cultured at 37 °C in 5% CO_2 in EBM-2 medium supplemented with hFGF (Lonza), genatmicin sulfate/amphotericin B (Lonza), Hepes 1 mM buffer (Lonza), fetal calf serum (Gibco), and hydrocortisone.

Nanoparticle Uptake Experiments by Flow Cytometry. Before each experiment cells were counted and resuspended in an appropriate volume of cMEM to obtain the required cell density. For flow cytometry, 2.5×10^5 cells were seeded into individual tissue 60 mm culture dishes (Greiner Bio-one) and incubated for 24 h prior to exposure to the nanoparticle suspension. Before exposure to nanoparticles, the cMEM was removed; then cells were washed once with PBS buffer prior to the addition of the nanoparticle dispersions. Nanoparticle dispersions were prepared by diluting the nanoparticle stock to the required concentration in SF or cMEM just before addition to cells.

For assessment of nanoparticle uptake levels by flow cytometry, after exposure to cells for the required time, the nanoparticle suspension was removed; then the cells were washed three times with PBS buffer and harvested with trypsin/EDTA for 3 min. Cells were fixed with 4% formaline solution (Sigma) for 20 min and then resuspended in PBS buffer for flow cytometry measurements.

For experiments at 4 °C, cells were preincubated for at least 30 min at 4 °C prior to the addition of the nanoparticle dispersion. To deplete the cell energy, a preincubation in 5 mg/mL sodium azide in cMEM was performed, followed by incubation with the nanoparticles in SF, also in sodium azide.

To expose the cells to the hard corona nanoparticle complexes in SF, 50 nm silica nanoparticles (250 μg/mL) were incubated with serum at 37 °C for 1 h; then the dispersions were centrifuged at 18 000 rcf at 15 °C for 40 min, in order to remove excess proteins and loosely bound proteins. The supernatant was discarded and the pellet was resuspended in PBS,

followed by a second centrifugation step at 18 000 rcf, 15 °C, for 20 min in order to leave on the nanoparticle surface only the proteins with higher affinities for the nanoparticles. The pellet was then redispersed in SF to a final concentration of 25 μg/mL prior to exposure to cells and assessment of uptake kinetics by flow cytometry as described above.

To compare the uptake levels in the different cell lines, all the cells, cultured as detailed above, were exposed for 1 h to the same nanoparticle dispersion in cMEM or SF, followed by cell fluorescence assessment by flow cytometry.

Flow cytometry fluorescence levels in the cells were measured using an Accuri C6 flow cytometer (Cambridgeshire, UK). Results are presented as the averaged mean of the cell fluorescence intensity distributions obtained by counting a minimum of 15 000 cells for each replica. Error bars are obtained by measuring the standard deviation among the replicates ($n = 3$).

Electron Microscopy. For electron microscopy, A549 cells treated as described above were fixed at room temperature in 2.5% glutaraldehyde in 0.1 M Sorensen phosphate buffer (pH 7.3) for 1 h, rinsed with Sorensen phosphate buffer (pH 7.3), and then postfixed for 1 h in 1% osmium tetroxide in deionized water. After the postfixation in some cases the cells have been treated overnight with a solution of uranyl acetate 2% w/w in distilled water to enhance the contrast of the membranes (examples are shown in Figure 3A−D). After dehydration in increasing concentrations of ethanol (from 70% up to 100%), the samples were immersed in an ethanol/Epon (1:1 vol/vol) mixture for 1 h before being transferred to pure Epon and embedded at 37 °C for 2 h. The final polymerization was carried out at 60 °C for 24 h. Ultrathin sections of 80 nm, obtained with a diamond knife using a Leica U6 ultramicrotome, were mounted on copper grids and stained with uranyl acetate and lead citrate (or lead citrate only in the case of pretreatment with uranyl acetate) before being examined with an FEI TECNAI transmission electron microscope.

Confocal Microscopy and Immunostaining. For confocal imaging, cells were plated on 35 mm plates with 15 mm diameter glass coverslips, at cell densities ranging from 1.25×10^5 to 1.8×10^5 cells per plate, and treated as described for flow cytometry sample preparation. For lysosomal or endosomal staining, samples were washed three times with PBS buffer, fixed for 20 min with 4% formaline, permeabilized for 5 min in 0.1% saponin from *Quillaja* bark (Sigma), and incubated for 30 min at room temperature with a blocking solution of 1% bovine albumin (Sigma) in PBS, to prevent nonspecific binding. Samples were then incubated for 1 h at room temperature with a primary antibody 1:200 mouse mAb to LAMP1 or EEA1 (Abcam, Cambrige, UK), washed three times with PBS buffer, and then incubated at room temperature for 1 h with a 1:400 dilution of AlexaFluor 647 goat anti-mouse IgG (H+L) as a secondary antibody (Molecular Probes). Samples were washed three times with PBS buffer and incubated for 5 min with DAPI (Sigma) before mounting with MOWIOL (Dako) on glass slides for imaging. The cells were observed using a Carl Zeiss LSM 510 Meta laser scanning confocal microscope (Zeiss, München, Germany) with lasers at 364 nm (DAPI), 488 nm (green-labeled nanoparticles), and 633 (LAMP1, EEA1 antibody).

ATP Assay. Intracellular levels of adenosine triphosphate (ATP) were quantified with the CellTiter-Glo luminescent cell viability assay (Promega Corporation, USA) according to the manufacturer's recommendations. Relative luminescent units (RLU) were detected with a Varioskan Flash plate reader (Thermo Scientific). The RLU values of cells treated with different concentrations of nanoparticles in cMEM and SF have been normalized to that of untreated cells in the same conditions.

Isolation and Characterization of the Hard Corona in Serum-Free and Complete Medium. The hard corona proteins recovered from the nanoparticles incubated with cells in SF and cMEM were compared by separation using SDS-PAGE gel electrophoresis (sodium dodecyl sulfate polyacrylamide gel electrophoresis). Nanoparticle dispersions in SF and cMEM were prepared as previously described. A549 cells were cultured as described above; then the cMEM was removed, the cells were washed once with PBS buffer, and the nanoparticle suspension in SF or cMEM was added. Cells were incubated with 100 μg/mL nanoparticles for 1 h in the two conditions; then the supernatant was collected to isolate hard corona proteins present after contact with cells on the recovered nanoparticles. As a control, cells were incubated with SF (or cMEM) medium for 1 h; then the supernatant was collected and incubated with silica nanoparticles (100 μg/mL) for 1 h prior to hard corona isolation. All the recovered dispersions were subjected to centrifugation at 20 000 rcf at 4 °C for 30 min, in order to remove excess proteins and loosely bound proteins. The supernatant was discarded, and the pellet was resuspended in 500 μL of filtered PBS. This step was repeated twice, followed by a third centrifugation step at 20 000 rcf, 4 °C, for 30 min in order to leave on the nanoparticle surface only the proteins with highest affinities for the nanoparticles (hard corona proteins). Finally after the last centrifugation, the pellet was resuspended carefully with 12 μL of PBS buffer and 6 μL of SDS−loading buffer (SDS + DTT, 9:1 volume). All samples were incubated for 5 min at 100 °C to denature the proteins, cooled to room temperature, and finally loaded into a 4% stacking gel with a 10% resolving gel and subjected to electrophoresis at 130 V for about 80 min, until the proteins neared the end of the gel. The gels were stained the following day using the DAIICHI silver staining kit (Tokyo, Japan).

Proteomic Analysis. To identify the recovered proteins by mass spectrometry, after separation by SDS-PAGE as described above, gel was stained using Coomassie Blue staining; then the bands of interest were excised from the gel and digested in-gel with trypsin (porcine trypsine, Promega), according to the method of Shevchenko *et al.*[47] The resulting peptide mixtures were resuspended in 0.1% formic acid and analyzed by electrospray liquid chromatography mass spectrometry (LC MS/MS) using an HPLC (Surveyor, ThermoFinnigan, CA, USA) interfaced with an LTQ Orbitrap (ThermoFinnigan). Chromatography buffer solutions (buffer A, 0.1% formic acid; buffer B, 100% acetonitrile and 0.1% formic acid) were run using a 72 min gradient. A flow rate of 150 μL/min was used at the electrospray source. Spectra were analyzed with Bioworks Browser 3.3.1 SP1 (ThermoFisher Scientific) using the Sequest Uniprot/Swiss-Prot database (www.expasy.org). The data have been searched against human and bovine protein databases in order to identify both the human cellular proteins present in the corona on the nanoparticles and the composition of the corona of the particles exposed to cells in the presence of bovine calf serum (cMEM), respectively. An exclusion filter was applied to reduce false positives, where peptides with $p < 0.005$ and X correlation scores of 1.9, 2, 2.5, and 3, for singly, doubly, and triply charged peptides, were retained. Multiconsensus analysis was performed when proteins with the same accession number were detected in multiple bands from the same sample: in these cases, their spectral counts were summed to get the total protein amount in the sample. Tables of the most abundant proteins identified, in this way, on nanoparticles exposed to cells in SF and cMEM conditions are given in the main text and in the Supporting Information. The complete mass spectrometry results are also provided in the Supporting Information as an additional file. This file is organized into four separate data sheets, containing the full list of proteins identified on the particles recovered from cells exposed in SF and cMEM conditions, each analyzed against both the human and the bovine database for completeness. The identified proteins have been ordered according to their abundance as described above.

Conflict of Interest: The authors declare no competing financial interest.

Acknowledgment. This work was conducted under the framework of the INSPIRE Programme, funded by the Irish Government's Programme for Research in Third Level Institutions, Cycle 4, National Development Plan 2007−2013 (A.S., M.P.M.) and is based upon works supported by the Small Collaborative Project NeuroNano funded by the European Commission Seventh Framework Programme (NNP4-SL-2008-214547) (A.L.). Additional financial support was provided by an EPA project grant (2008–EH-MS-5-S3-R2) (F.F.) and the Irish Research Council for Science, Engineering and Technology (C.Å.). D. Cottell is kindly acknowledged for help in the interpretation of the electron microscopy results.

Use of the UCD Conway Flow Cyotmetry, Imaging and Electron Microscopy Facilities and of the UCD Conway Mass Spectrometry Resource is also acknowledged.

Supporting Information Available: Additional data on the uptake of both silica and polystyrene particles in serum-free conditions in different cell lines and the proteins found in the corona on the nanoparticles are presented. A separate file containing a full list of proteins identified by mass spectrometry analysis on the nanoparticles exposed to cells in SF and cMEM conditions is also included. This material is available free of charge *via* the Internet at http://pubs.acs.org.

REFERENCES AND NOTES

1. Salvati, A.; Åberg, C.; dos Santos, T.; Varela, J.; Pinto, P.; Lynch, I.; Dawson, K. A. Experimental and Theoretical Comparison of Intracellular Import of Polymeric Nanoparticles and Small Molecules: Towards Models of Uptake Kinetics. *Nanomedicine Nanotechnol. Biol. Med.* **2011**, *7*, 818–826.
2. Jiang, W.; Kim, B. Y. S.; Rutka, J. T.; Chan, W. C. W. Nanoparticle-Mediated Cellular Response is Size-Dependent. *Nat. Nanotechnol.* **2008**, *3*, 145–150.
3. Gratton, S. E. A.; Ropp, P. A.; Pohlhaus, P. D.; Luft, J. C.; Madden, V. J.; Napier, M. E.; DeSimone, J. M. The Effect of Particle Design on Cellular Internalization Pathways. *Proc. Natl. Acad. Sci. U. S. A.* **2008**, *105*, 11613–11618.
4. Oberdörster, G. Safety Assessment for Nanotechnology and Nanomedicine: Concepts of Nanotoxicology. *J. Intern. Med.* **2010**, *267*, 89–105.
5. Rejman, J.; Oberle, V.; Zuhorn, I. S.; Hoekstra, D. Size-Dependent Internalization of Particles *via* the Pathways of Clathrin- and Caveolae-Mediated Endocytosis. *Biochem. J.* **2004**, *377*, 159–169.
6. Conner, S. D.; Schmid, S. L. Regulated Portals of Entry into the Cell. *Nature* **2003**, *422*, 37–44.
7. Mayor, S.; Pagano, R. E. Pathways of Clathrin-Independent Endocytosis. *Nat. Rev. Mol. Cell Biol.* **2007**, *8*, 603–612.
8. Lu, J.; Liong, M.; Sherman, S.; Xia, T.; Kovochich, M.; Nel, A.; Zink, J.; Tamanoi, F. Mesoporous Silica Nanoparticles for Cancer Therapy: Energy-Dependent Cellular Uptake and Delivery of Paclitaxel to Cancer Cells. *NanoBiotechnology* **2007**, *3*, 89–95.
9. Shapero, K.; Fenaroli, F.; Lynch, I.; Cottell, D. C.; Salvati, A.; Dawson, K. A. Time and Space Resolved Uptake Study of Silica Nanoparticles by Human Cells. *Mol. BioSyst.* **2011**, *7*, 371–378.
10. Kim, J.-S.; Yoon, T.-J.; Yu, K.-N.; Noh, M. S.; Woo, M.; Kim, B.-G.; Lee, K.-H.; Sohn, B.-H.; Park, S.-B.; Lee, J.-K.; *et al*. Cellular Uptake of Magnetic Nanoparticle Is Mediated through Energy-Dependent Endocytosis in A549 Cells. *J. Vet. Sci.* **2006**, *7*, 321–326.
11. Xing, X.; He, X.; Peng, J.; Wang, K.; Tan, W. Uptake of Silica-Coated Nanoparticles by HeLa Cells. *J. Nanosci. Nanotechnol.* **2005**, *5*, 1688–1693.
12. Doherty, G. J.; McMahon, H. T. Mechanisms of Endocytosis. *Annu. Rev. Biochem.* **2009**, *78*, 857–902.
13. Cedervall, T.; Lynch, I.; Lindman, S.; Berggard, T.; Thulin, E.; Nilsson, H.; Dawson, K. A.; Linse, S. Understanding the Nanoparticle-Protein Corona Using Methods to Quantify Exchange Rates and Affinities of Proteins for Nanoparticles. *Proc. Natl. Acad. Sci. U. S. A.* **2007**, *104*, 2050–2055.
14. Röcker, C.; Potzl, M.; Zhang, F.; Parak, W. J.; Nienhaus, G. U. A Quantitative Fluorescence Study of Protein Monolayer Formation on Colloidal Nanoparticles. *Nat. Nanotechnol.* **2009**, *4*, 577–580.
15. Casals, E.; Pfaller, T.; Duschl, A.; Oostingh, G. J.; Puntes, V. Time Evolution of the Nanoparticle Protein Corona. *ACS Nano* **2010**, *4*, 3623–3632.
16. Lynch, I.; Salvati, A.; Dawson, K. A. Protein-Nanoparticle Interactions: What Does the Cell See? *Nat. Nanotechnol.* **2009**, *4*, 546–547.
17. Walczyk, D.; Baldelli Bombelli, F.; Monopoli, M.; Lynch, I.; Dawson, K. A. What the Cell "Sees" in Bionanoscience. *J. Am. Chem. Soc.* **2010**, *132*, 5761–5768.
18. Monopoli, M. P.; Baldelli Bombelli, F.; Dawson, K. A. Nanobiotechnology: Nanoparticle Coronas Take Shape. *Nat. Nanotechnol.* **2011**, *6*, 11–12.
19. Monopoli, M. P.; Walczyk, D.; Campbell, A.; Elia, G.; Lynch, I.; Baldelli Bombelli, F.; Dawson, K. A. Physical-Chemical Aspects of Protein Corona: Relevance to *in Vitro* and *in Vivo* Biological Impacts of Nanoparticles. *J. Am. Chem. Soc.* **2011**, *133*, 2525–2534.
20. Nel, A. E.; Madler, L.; Velegol, D.; Xia, T.; Hoek, E. M. V.; Somasundaran, P.; Klaessig, F.; Castranova, V.; Thompson, M. Understanding Biophysicochemical Interactions at the Nano-Bio Interface. *Nat. Mater.* **2009**, *8*, 543–557.
21. Rivera Gil, P.; Oberdörster, G.; Elder, A.; Puntes, V.; Parak, W. J. Correlating Physico-Chemical with Toxicological Properties of Nanoparticles: The Present and the Future. *ACS Nano* **2010**, *4*, 5527–5531.
22. Xia, X.-R.; Monteiro-Riviere, N. A.; Riviere, J. E. An Index for Characterization of Nanomaterials in Biological Systems. *Nat. Nanotechnol.* **2010**, *5*, 671–675.
23. Zhu, Y.; Li, W.; Li, Q.; Li, Y.; Li, Y.; Zhang, X.; Huang, Q. Effects of Serum Proteins on Intracellular Uptake and Cytotoxicity of Carbon Nanoparticles. *Carbon* **2009**, *47*, 1351–1358.
24. Patel, P. C.; Giljohann, D. A.; Daniel, W. L.; Zheng, D.; Prigodich, A. E.; Mirkin, C. A. Scavenger Receptors Mediate Cellular Uptake of Polyvalent Oligonucleotide-Functionalized Gold Nanoparticles. *Bioconjugate Chem.* **2010**, *21*, 2250–2256.
25. Bajaj, A.; Samanta, B.; Yan, H.; Jerry, D. J.; Rotello, V. M. Stability, Toxicity and Differential Cellular Uptake of Protein Passivated-Fe_3O_4 Nanoparticles. *J. Mater. Chem.* **2009**, *19*, 6328–6331.
26. Stayton, I.; Winiarz, J.; Shannon, K.; Ma, Y. Study of Uptake and Loss of Silica Nanoparticles in Living Human Lung Epithelial Cells at Single Cell Level. *Anal. Bioanal. Chem.* **2009**, *394*, 1595–1608.
27. Guarnieri, D.; Guaccio, A.; Fusco, S.; Netti, P. Effect of Serum Proteins on Polystyrene Nanoparticle Uptake and Intracellular Trafficking in Endothelial Cells. *J. Nanopart. Res.* **2011**, *13*, 4295–4309.
28. Ehrenberg, M. S.; Friedman, A. E.; Finkelstein, J. N.; Oberdörster, G.; McGrath, J. L. The Influence of Protein Adsorption on Nanoparticle Association with Cultured Endothelial Cells. *Biomaterials* **2009**, *30*, 603–610.
29. Jiang, X.; Weise, S.; Hafner, M.; Röcker, C.; Zhang, F.; Parak, W. J.; Nienhaus, G. U. Quantitative Analysis of the Protein Corona on FePt Nanoparticles Formed by Transferrin Binding. *J. R. Soc., Interface* **2010**, *7*, S5–S13.
30. Iversen, T.-G.; Skotland, T.; Sandvig, K. Endocytosis and Intracellular Transport of Nanoparticles: Present Knowledge and Need for Future Studies. *Nano Today* **2011**, *6*, 176–185.
31. dos Santos, T.; Varela, J.; Lynch, I.; Salvati, A.; Dawson, K. A. Effects of Transport Inhibitors on the Cellular Uptake of Carboxylated Polystyrene Nanoparticles in Different Cell Lines. *PLoS ONE* **2011**, *6*, e24438.
32. Ge, C.; Du, J.; Zhao, L.; Wang, L.; Liu, Y.; Li, D.; Yang, Y.; Zhou, R.; Zhao, Y.; Chai, Z.; *et al*. Binding of Blood Proteins to Carbon Nanotubes Reduces Cytotoxicity. *Proc. Natl. Acad. Sci. U. S. A.* **2011**, *108*, 16968–16973.
33. Hu, W.; Peng, C.; Lv, M.; Li, X.; Zhang, Y.; Chen, N.; Fan, C.; Huang, Q. Protein Corona-Mediated Mitigation of Cytotoxicity of Graphene Oxide. *ACS Nano* **2011**, *5*, 3693–3700.
34. Shi, J.; Karlsson, H. L.; Johansson, K.; Gogvadze, V.; Xiao, L.; Li, J.; Burks, T.; Garcia-Bennett, A.; Uheida, A.; Muhammed, M.; *et al*. Microsomal Glutathione Transferase 1 Protects against Toxicity Induced by Silica Nanoparticles but Not by Zinc Oxide Nanoparticles. *ACS Nano* **2012**, *6*, 1925–1938.
35. Haniu, H.; Saito, N.; Matsuda, Y.; Kim, Y. A.; Park, K. C.; Tsukahara, T.; Usui, Y.; Aoki, K.; Shimizu, M.; Ogihara, N.; *et al*. Effect of Dispersants of Multi-Walled Carbon Nanotubes on Cellular Uptake and Biological Responses. *Int. J. Nanomed.* **2011**, *6*, 3295–307.
36. Dutta, D.; Sundaram, S. K.; Teeguarden, J. G.; Riley, B. J.; Fifield, L. S.; Jacobs, J. M.; Addleman, S. R.; Kaysen, G. A.; Moudgil, B. M.; Weber, T. J. Adsorbed Proteins Influence

the Biological Activity and Molecular Targeting of Nanomaterials. *Toxicol. Sci.* **2007**, *100*, 303–315.
37. Lunov, O.; Syrovets, T.; Loos, C.; Beil, J.; Delacher, M.; Tron, K.; Nienhaus, G. U.; Musyanovych, A.; Mailänder, V.; Landfester, K.; *et al*. Differential Uptake of Functionalized Polystyrene Nanoparticles by Human Macrophages and a Monocytic Cell Line. *ACS Nano* **2011**, *5*, 1657–1669.
38. Kobzik, L. Lung Macrophage Uptake of Unopsonized Environmental Particulates. Role of Scavenger-Type Receptors. *J. Immunol.* **1995**, *155*, 367–76.
39. Hamilton, R. F.; Thakur, S. A.; Mayfair, J. K.; Holian, A. MARCO Mediates Silica Uptake and Toxicity in Alveolar Macrophages from C57BL/6 Mice. *J. Biol. Chem.* **2006**, *281*, 34218–34226.
40. Lesniak, A.; Campbell, A.; Monopoli, M.; Lynch, I.; Salvati, A.; Dawson, K. A. Serum Heat Inactivation Affects Protein Corona Composition and Nanoparticle Uptake. *Biomaterials* **2010**, *31*, 9511–9518.
41. Tahara, K.; Sakai, T.; Yamamoto, H.; Takeuchi, H.; Hirashima, N.; Kawashima, Y. Improved Cellular Uptake of Chitosan-Modified PLGA Nanospheres by A549 Cells. *Int. J. Pharm.* **2009**, *382*, 198–204.
42. Kim, J. A.; Åberg, C.; Salvati, A.; Dawson, K. A. Role of Cell Cycle on the Cellular Uptake and Dilution of Nanoparticles in a Cell Population. *Nat. Nanotechnol.* **2012**, *7*, 62–68.
43. Choi, S.-J.; Oh, J.-M.; Choy, J.-H. Toxicological Effects of Inorganic Nanoparticles on Human Lung Cancer A549 Cells. *J. Inorg. Biochem.* **2009**, *103*, 463–471.
44. Huang, M.; Ma, Z.; Khor, E.; Lim, L.-Y. Uptake of FITC-Chitosan Nanoparticles by A549 Cells. *Pharm. Res.* **2002**, *19*, 1488–1494.
45. Lundqvist, M.; Stigler, J.; Elia, G.; Lynch, I.; Cedervall, T.; Dawson, K. A. Nanoparticle Size and Surface Properties Determine the Protein Corona with Possible Implications for Biological Impacts. *Proc. Natl. Acad. Sci. U. S. A.* **2008**, *105*, 14265–14270.
46. Cedervall, T.; Lynch, I.; Foy, M.; Berggård, T.; Donnelly, S. C.; Cagney, G.; Linse, S.; Dawson, K. A. Detailed Identification of Plasma Proteins Adsorbed on Copolymer Nanoparticles. *Angew. Chem., Int. Ed.* **2007**, *46*, 5754–5756.
47. Shevchenko, A.; Wilm, M.; Vorm, O.; Mann, M. Mass Spectrometric Sequencing of Proteins from Silver-Stained Polyacrylamide Gels. *Anal. Chem.* **1996**, *68*, 850–858.